Received: 31 December 2020 | Revised: 19 April 2021 | Accepted: 12 May 2021

DOI: 10.1002/cli2.7

Climate Resilience and Sustainability
Interdisciplinary Approaches Towards Solutions for Climate Change
Open Access
RMetS

RESEARCH ARTICLE

Importance of including soil moisture in drought monitoring over the Brazilian semiarid region: An evaluation using the JULES model, in situ observations, and remote sensing

Marcelo Zeri[1] | **Karina Williams**[2,6] | **Ana Paula M. A. Cunha**[1] | **Gisleine Cunha-Zeri**[5] | **Murilo S. Vianna**[4] | **Eleanor M. Blyth**[3] | **Toby R. Marthews**[3] | **Garry D. Hayman**[3] | **José Maria Costa**[1] | **José A. Marengo**[1] | **Regina C. S. Alvalá**[1] | **Osvaldo L. L. Moraes**[1] | **Marcelo V. Galdos**[4]

[1] National Center for Monitoring and Early Warning of Natural Disasters (Cemaden), São José dos Campos, São Paulo, Brazil

[2] Met Office, Exeter, UK

[3] UK Centre for Ecology & Hydrology (UKCEH), Wallingford, UK

[4] School of Earth and Environment, University of Leeds, Leeds, UK

[5] National Institute for Space Research (INPE), São José dos Campos, São Paulo, Brazil

[6] Global Systems Institute, University of Exeter, Exeter, UK

Correspondence
Marcelo Zeri, National Center for Monitoring and Early Warning of Natural Disasters (Cemaden), São José dos Campos, SP 12247-016, Brazil.
Email: marcelo.zeri@cemaden.gov.br

Funding information
Coordination for the Improvement of Higher Education Personnel (CAPES), Grant/Award Number: 88887.308408/2018-00; Newton Fund, Grant/Award Number: DN373701

Abstract

Soil moisture information is essential to monitoring of the intensity of droughts, the start of the rainy season, planting dates and early warnings of yield losses. We assess spatial and temporal trends of drought over the Brazilian semiarid region by combining soil moisture observations from 360 stations, root zone soil moisture from a leading land surface model, and a vegetation health index from remote sensing. The soil moisture dataset was obtained from the network of stations maintained by the National Center of Monitoring and Early Warning of Natural Disasters (Cemaden), in Brazil. Soil water content at 10 to 35 cm depth, for the period 1979–2018, was obtained from running the JULES land surface model (the Joint UK Land Environment Simulator). The modelled soil moisture was correlated with measurements in the common period of 2015–2018, resulting in an average correlation coefficient of 0.48 across the domain. The standardized soil moisture anomaly (SMA) was calculated for the long-term modelled soil moisture and revealed strong negative values during well-known drought periods in the region, especially during El-Niño years. The performance of SMA in identifying droughts during the first 2 months of the raining and cropping season was similar to the Standardized Precipitation Index (SPI), commonly used for drought assessment: 12–14 events were identified by both indices. Finally, the temporal relationship between both SMA and SPI with the Vegetation Health Index (VHI) was assessed using the cross-wavelet transform. The results indicated lagged correlations of 1 to 1.5 months in the annual scale, suggesting that negative trends in SMA and SPI can be an early warning to yield losses during

the growing season. Public policies on drought assessment should consider the combination of multiple drought indices, including soil moisture anomaly.

KEYWORDS
drought, drought indices, drought management policies, land surface model, soil moisture

1 | INTRODUCTION

Drought is a natural disaster characterized by a slow onset and evolution (Marthews et al., 2019; Mishra & Singh, 2010; van Loon, 2015). The impacts of droughts are experienced in several societal sectors and activities, such as agriculture, water supply, food security, tourism and energy generation (Mishra & Singh, 2010). Droughts can be recurrent in specific regions of the world, but every event has unique characteristics regarding the duration and intensity. The influence of climate on drought occurrence and recurrence is currently an uncertain issue considering the spatial and temporal variabilities caused by climate change (Trenberth et al., 2014). Therefore, monitoring of drought conditions is a crucial and timely task, which is essential to mitigate the impacts of recurrent and unexpected events (Wilhite, 2018). For this reason, the improvement of existing drought monitoring tools and testing of new approaches should be carried out continuously (Svoboda & Fuchs, 2017).

The Brazilian semiarid region (Figure 1) is subject to frequent droughts, with famine and migrations associated with events since the 18th century (De Alcântara Silva et al., 2013; Gonçalves, 2000; Rossato et al., 2017). The region covers approximately 18% of the territory of Brazil and has 22 million inhabitants (IBGE, 2019a). Droughts in the region are typically assumed to be linked to El Niño events; however, the period 2012 to 2018 was characterized by strong annual droughts which were not associated with El Niño, except 2015/2016 (Cunha et al., 2019; de Souza et al., 2005; Hastenrath & Heller, 1977; Pezzi & Cavalcanti, 2001). In addition, due to the region's latitudinal extent, drought events affect different parts of the domain with varying degrees of severity. According to reports on the history of droughts in the region, the spatial patterns of drought impacts is not always the same and has been changing in recent years, with stronger trends towards drier conditions (Cunha et al., 2018; Tomasella et al., 2018).

Drought is the main manifestation of climate change and variability in the semiarid region of northeast Brazil, which dramatically affects its rural and poor population (Simões et al., 2010). There are numerous risks and vulnerabilities brought about by droughts, besides water scarcity: decreased agricultural productivity, loss of income of rural population, risk of food insecurity and breakdown of food systems, impaired ecosystem diversity, with all that consequently influencing social and economic development and impacting on human health, particularly to poorer populations in urban and rural settings (FAO, 2017; Holmgren et al., 2006; Sena et al., 2018).

In this context, policymakers have to go beyond strategies that not only increase agricultural productivity but also integrate measures to mitigate the risks arising from climate variability and improve conditions for rural prosperity and poverty eradication (Hansen et al., 2019), as well as adaptation initiatives to support local populations to deal with drought risks in the future. According to Farinelli et al. (2017), the legal framework for drought management in the Brazilian semiarid region must include specific mitigation actions (adoption of sustainable agricultural practices and infrastructure for water management, for instance) and social protection programs (guaranteed minimum income, education, and health care). Unfortunately, governmental responses have historically been reactive other than proactive, that is, more focused on crisis management approach than on preparedness and drought risk reduction (Magalhaes, 2017; Wilhite et al., 2014).

In 2002, Brazil instituted the *Garantia Safra* benefit (Law number 10.420/2002), in the scope of the *National Program for Strengthening Family Farming—PRONAF* (Decree number 1.946/1996). The Garantia-Safra is an income insurance linked to agricultural production and targets poor and vulnerable smallholder farmers in drought-prone region, mostly in the northeast Brazil (Milhorance et al., 2020). Besides ensuring financial security for family farmers in the cultures they traditionally produce (basically cotton, rice, cassava, beans, and corn—the most traditional crops in the region), the program aims at promoting other feasible activities, such as the adoption of crops resistant to water shortage (Alves, 2009). The Garantia-Safra has limited action, as it lacks a preventive function and fails as an instrument to build farmers' long-term resilience and fight poverty that characterizes the region (Kühne, 2020).

Eligibility for the Garantia-Safra benefit includes (i) be a family farmer by meeting the PRONAF criteria, (ii) have a monthly family income of a maximum of 1.5 minimum wage, and (iii) plant between 0.6 to 5.0 hectares

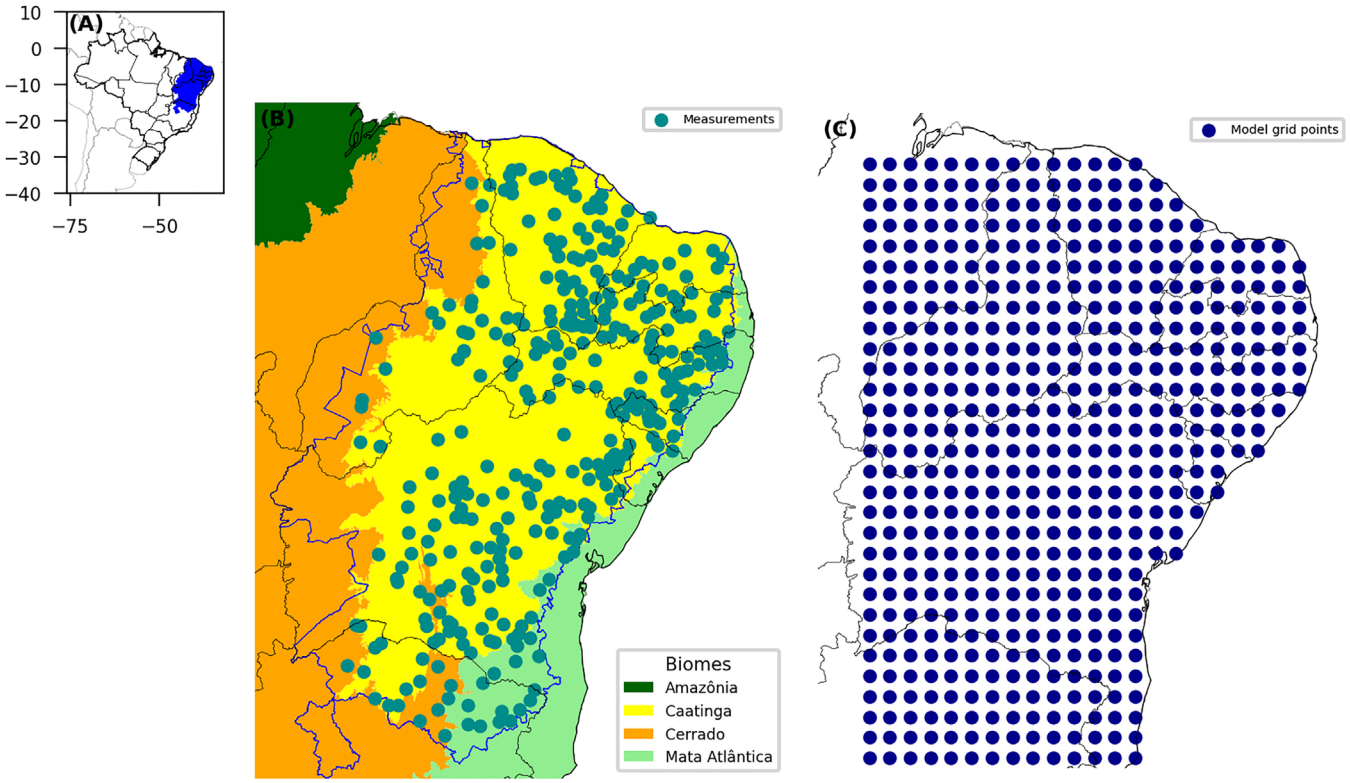

FIGURE 1 (a) Brazil and semiarid region (blue); (b) soil moisture measurement sites over the Brazilian semiarid region (blue contour); (c) grid points from the JULES model

of beans, corn, rice, cotton, and/or cassava. Additionally, there are verification instruments to assess the occurrence of drought and crop failure; such instruments encompass reports on on-site surveys, rainfall anomalies, and drought indices (MAPA, 2020). However, no information on soil moisture is currently used for the crop losses verification.

Drought can be monitored in several ways by making use of in situ sensors, via satellite products or using land surface models of water balance (Alvalá et al., 2019; Cunha et al., 2015; Zeri et al., 2018). Hybrid approaches make use of measurements to validate models of water balance (Cammalleri et al., 2015; Souza et al., 2021). A combined index making use of vegetation conditions (remote sensing), soil moisture (land surface model), and rainfall anomalies is used to estimate drought conditions in Europe (Carrão et al., 2016; Sepulcre-Canto et al., 2012). The challenge is to obtain an appropriate combination, which captures the different spatial and temporal characteristics of the processes causing drought (Wilhite, 2018). Meteorological drought is defined as a deficit in rainfall totals over a certain period. Longer periods of rainfall deficit result in agricultural drought affecting plant growth, livestock welfare, and ultimately the regional food security (Godfray et al., 2010). Finally, hydrological drought is the result of the impact of long-term rainfall deficit on reservoir and river levels (van Loon, 2015). A combined drought index should be composed of elements that capture all the spatial and temporal variability of rainfall, soil moisture and vegetation health, considering also delays between the individual components.

A combined drought index was proposed by Cao et al. (2019) in a case study over northeast China, making use of remote sensing data for soil moisture and precipitation, and calculation of Potential Evapotranspiration (PET). The Vegetation-Soil Water Deficit (VSWD), proposed in the study, was compared with other metrics such as the Vegetation Health Index (VHI) and the Standardized Precipitation-Evapotranspiration Index (SPEI). The VSWD was found to better represent the severities of drought based on in-situ verification; the performance was also superior when evaluating past drought events over the region.

Soil moisture from remote sensing has been recently included in the drought index generated by the National Center for Monitoring and Early Warning of Natural Disasters (Cemaden), in Brazil. The integrated drought index IIS (from *Índice Integrado de Seca*, in Portuguese) makes use of the Standardized Precipitation Index (SPI), VHI, and Root Zone Soil Moisture (RZSM) from NASA's GRACE satellite mission. Each individual index is converted to classes of drought (1 to 5, from severe to light, and 6, for normal conditions). The index is calculated as an average of the

three reclassed indices and published monthly in drought reports on Cemaden's website (www.cemaden.gov.br). The RZSM was not included in the current work due to the shorter data coverage (starting in 2003), as compared with the 1979–2018 soil moisture modelled run and rainfall data for SPI.

The objective of this study is to investigate the spatial and temporal variability of soil moisture conditions in the Brazilian semiarid using soil moisture observation and simulations by the JULES land surface model. To test whether soil moisture can be complementary to current drought indices and indicators, long-term anomalies of soil moisture were compared to anomalies of a vegetation index, which can be a proxy to drought impacts such as crop yield losses. The temporal relationship between the soil moisture anomaly and the vegetation index was investigated using the cross-wavelet transform, enabling the identification of temporal lags between the time series. Negative anomalies in soil moisture related to future negative anomalies in the vegetation index can be used as early warning of drought impacts. Results from this work could support the integration of soil moisture estimates into national initiatives of drought monitoring.

2 | SITE AND METHODOLOGY

2.1 | Measurements sites

The site locations are shown in Figure 1, as well as the official delimitation of the Brazilian semiarid region (blue contour), and the dominant biome over this area, the Caatinga, a seasonally dry tropical forest characterized by shrubs and thorny tree species (IBGE, 2019b). The region is mostly characterized by sandy soils (Dijkshoorn et al., 2005; Zeri et al., 2018). Annual rainfall ranges from 200 to 800 mm·year^{-1} and is highly influenced by patterns of Sea Surface Temperature (SST) in the tropical Pacific (El Niño/Southern Oscillation—ENSO) and Atlantic Oceans. The rainy season in some parts of northeast Brazil starts in October/November and ends in July, depending on the location. Rainfall over the southern part starts in October/November and is associated with the passage of fronts from the south; the position of the Intertropical Convergence Zone (ITCZ) influences rainfall variability over the northern part, where precipitation starts in January/February and peaks in March–May. For regions close to the coast, the rainy season occurs from April to July (Cavalcanti, 2009; Kousky, 1979).

Stations were installed between 2014 and 2015 within the semiarid region (Figure 1b) as part of Cemaden's efforts to monitor precipitation and soil moisture over the region most affected by droughts in Brazil. Soil moisture probes (EC-5 model, Decagon Devices, Pullman, WA, USA) making continuous measurements of volumetric water content (in m^3 m^{-3}) at soil depths of 10 and 20 cm were installed at each station. The stations are also equipped with rain gauges (model PluvDB, DualBase, Santa Catarina, Brazil). The network now has 595 stations over 9 states, most of them installed at rural properties of subsistence agriculture. Typical crops include rainfed maize and beans. Example applications of the measurements carried out using this network can be found in a previous study (Zeri et al., 2018).

The dataset used in the current study comprises of a subset of stations selected based in a quality control process, which was recently made available (Zeri et al., 2020). The dataset contains measurements from 360 stations with at least 2 consecutive months of data, showing physically consistent values in comparison with other depths. Soil moisture values were considered acceptable within the range of 0 to 0.8 m^3 m^{-3}. The majority of stations had measurements at 10 and 20 cm, which were averaged (depths) for the correlation with modelled values.

2.2 | JULES land surface model

We use the JULES land surface model (Best et al., 2011; Clark et al., 2011), a community model developed in the UK. JULES is a process-based simulator of the exchange of water, energy and carbon between the land surface and atmosphere. It can operate as a standalone land surface model with driving meteorology or as the land surface component of UK numerical weather prediction, chemistry-climate and Earth system models (Marthews et al., 2012; Sellar et al., 2020; Walters et al., 2014).

JULES uses 4 soil layers, with thicknesses 0.1, 0.25, 0.65, and 2 m (i.e., total depth of soil column is 3 m) and the soil moisture is updated on an hourly timestep. The vertical fluxes of water between layers follow Darcy's Law. Precipitation can be intercepted and stored by the plant canopy. The water reaching the surface is partitioned into infiltration and surface runoff. Water is removed from the soil layers by plant transpiration and by evaporation from the top soil level (and also to prevent supersaturation). Stomatal conductance is calculated from net leaf photosynthesis, which uses the parametrisation from Collatz et al. (1991) for C3 plants and Collatz et al. (1992) for C4 plants. Leaf photosynthesis is moderated by a soil moisture stress term. The contribution of different soil layers to this overall soil moisture stress term depends on an exponential distribution, with a decay constant related to the effective root depth of the plant functional type. The canopy radiation scheme is multi-layer and includes sunflecks. Subsurface runoff is calculated using a TOPMODEL approach, which simulates the height of the saturated zone in the soil

column and an additional deep soil layer (this deep layer has thickness 3 m and an exponential decay of saturated hydraulic conductivity with depth).

The soil moisture is modelled for the entire gridbox (i.e., not for each tile type separately). We would expect to see an improvement if the model was instead run at individual sites, with soil properties measured at each site, and the site landcover. The Plant Functional Types (PFTs) and land cover used are shown in Figure S1, Supporting Information.

Soil moisture in JULES has been evaluated against in situ soil moisture data (e.g., Iwema et al., 2017) and soil moisture satellite products (Schellekens et al., 2017). Other parts of the simulation that are influenced by absolute soil moisture or soil moisture anomalies, such as evapotranspiration, water stress, runoff, water table depth have also been evaluated in recent years (Blyth et al., 2011; Ellis et al., 2009; Haddeland et al., 2011; Martínez-de la Torre et al., 2019; Pan et al., 2020; Paschalis et al., 2020; Ukkola et al., 2016).

In this study, we use JULES in standalone mode, driven with the global WFDEI meteorological forcing data (WATCH Forcing Data methodology applied to ERA-Interim data (Weedon et al., 2014). The JULES version is revision 9061 (which is between the tagged releases 4.9 and 5.0). For more information about the model setup for these runs, see Bett et al. (2020).

A global gridded run at 0.5° x 0.5° spatial resolution was undertaken for the years 1979 to 2018. The variables of interest (e.g., modelled soil moisture as a function of soil depth) were extracted for a domain covering northeast Brazil (46°W-32°W, 18°S-3°S). We use the standard set of soil ancillary parameters. The variable used was the one corresponding to the soil water content at 10 to 35 cm depth. The depth of 35 cm is within the root zone of maize, the most commonly rainfed crop planted over the subsistence agriculture farms in the region.

2.3 | Long-term anomalies of rainfall, vegetation index, and soil moisture

Anomalies of rainfall, a satellite vegetation index, and soil moisture were calculated using the same approach commonly used to calculate the SPI. The SPI is proportional to a z-score, that is, a measure of standard deviations above the long-term mean. Other approaches used to calculate anomalies include percentiles over a long-term mean, in addition to the use of different time scales for SPI, such as every 3, 6 or 12 months. In this study, 1-month SPI was chosen as to have a unified approach to the anomalies of the three components: rainfall (SPI), VHI, and soil moisture.

The choices of SPI and VHI are justified due to their relatively simple calculation and few data requirements. SPI is adequate to Brazilian conditions since it requires only measurements of rainfall. The SPI can be calculated using gridded datasets of rainfall, in addition to in-situ measurements. Other indices such as the Standardized Precipitation Evapotranspiration Index (SPEI) or Palmer Drought Severity Index (PDSI), for soil moisture, require additional measurements of evapotranspiration or soil moisture, among other variables, which are not common to find in several regions in Brazil (Svoboda & Fuchs, 2017; Vicente-Serrano et al., 2010). An assessment of the performance of SPI, VHI, and a soil moisture anomaly supports their current use in Brazilian drought monitoring initiatives and help to improve its accuracy.

2.3.1 | Standardized Precipitation Index

The anomaly of rainfall is derived from the calculations of the SPI, which converts monthly totals of precipitation into a range of values from -2 to 2, approximately equal to a number of standard deviations from the mean (McKee et al., 1993, 1995). The SPI is the most commonly used index for monitoring of meteorological drought (Svoboda & Fuchs, 2017). For its calculation, the time series is fitted to a gamma distribution, usually reported to be appropriate to describe rainfall records (Alam et al., 2018; Lima et al., 2021; Thom, 1958; Yuan et al., 2018). The whole record of rainfall (1981–2020) was used for the fitting process. Next, the gamma cumulative distribution function (CDF) is calculated with the resulting parameters from the fit. Finally, the value of SPI is derived from the transformation of the CDF into a normal distribution.

A drought event is ongoing when SPI falls below a threshold, usually -1, during a certain period. The index can be calculated for different time scales, such as monthly, 3-monthly, yearly, and so on. In this work, we utilized the monthly scale so that drought could be estimated in specific months of the crop calendar in each region. SPI was calculated using an implementation in Python, already applied in a study of rainfall variability over Central Brazil (Zeri et al., 2019).

Rainfall data for the calculation of SPI was obtained from CHIRPS, a global collection of precipitation records interpolated over a 0.05 degree grid (Funk et al., 2014). This dataset has been evaluated over Brazilian regions before, resulting in different performances over the biomes (Cavalcante et al., 2020; Paredes-Trejo et al., 2017). A study using 21 rainfall stations over the Brazilian northeast resulted in good correlation with CHIRPS ($r = 0.94$), but overestimation and underestimation reported for the low and high extremes of rainfall (Paredes-Trejo et al., 2017).

According to the authors, uncertainties can be higher than 100 mm/month when comparing estimates from CHIRPS and stations. An evaluation of rainfall products (CHIRPS, TRMM, ETA model) against weather stations over Minas Gerais state found good agreement of CHIRPS with measurements, with coefficient of determination (r^2) and Nash-Sutcliffe efficiency coefficient (EFF) both higher than 0.9 (Nogueira et al., 2018). However, it should be noted that the study was not focused on the semiarid part of Minas Gerais, but rather on the south and southeastern parts of the state. Overall, uncertainty in rainfall estimates is expected over Brazil, especially over its northeast region, due to the poor spatial and temporal coverage of weather stations.

2.3.2 | Vegetation Health Index Anomaly

The VHI is a satellite product regarded as a proxy to thermal and moisture conditions over vegetated surfaces (Bokusheva et al., 2016; Kogan, 2002). VHI is a combination of two indices, the Vegetation Condition Index (VCI) and Temperature Condition Index (TCI), expressed as:

$$\mathrm{VHI} = 0.5 * \mathrm{VCI} + 0.5 * \mathrm{TCI} \quad (1)$$

where VCI is obtained by normalizing the NDVI (Normalized Difference Vegetation Index) from multi-year minimum and maximum values; and TCI is a proxy for thermal condition obtained by normalizing the brightness temperature (BT), also from multi-year minimum and maximum values (1982–2018). VHI ranges from 0 to 100, with values smaller than 40 indicating water stress condition, and greater than 40 indicating good conditions for vegetation (Kogan, 1995, 1997).

The composite VHI is provided every 7 days by the National Oceanic and Atmospheric Administration (NOAA). In this work, data from 1982 to 2018 was used. The 7-day releases were averaged monthly. Next, the anomaly of this index ($\mathrm{VHI_a}$) was estimated using the same approach used for the calculation of SPI.

2.3.3 | Standardized Soil Moisture Anomaly

Finally, the model data were used to calculate a Standardized Soil Moisture Anomaly (SMA). The index was calculated with the same approach used to generate the SPI of rainfall data, where the whole series is used to fit a gamma function, later converted to a normal distribution. The result is a monthly anomaly of soil moisture ranging from approximately -4 to 4, with negative values denoting drought. This approach is similar to the one used in a previous study, where soil moisture anomaly was calculated using a z-score (Xu et al., 2018).

Strong negative events of SMA were compared with episodes of ENSO from 1981 to 2018. The comparison used classifications based on the Oceanic Niño Index (ONI), developed by the National Oceanic and Atmospheric Administration (NOAA). The following classes of ENSO were considered: moderate, strong and very strong (Null, 2021). Episodes of ENSO are generally reported as a two-year event (e.g., 1997–1998), with a historical variability in start, end and duration. Here, the episodes were marked in Figure 3 ranging from January 1st of the first year until December 31st of the following year.

2.4 | Cross-wavelet analysis

Wavelet analysis is a signal processing tool used to identify frequencies, or harmonics, which are present in a time series and contribute to its variance over time (Grinsted et al., 2004; Torrence & Compo, 1998). The technique has the advantage of highlighting harmonics which are intermittent in time, which is a useful feature when analysing climate signals with low stationarity. A time series is considered to have low stationarity when its statistical moments (mean, variance, skewness, kurtosis) change significantly over time (Wilks, 1995). Geophysical time series, specifically climate data, usually are subjected to intermittent influences which are easily identified in wavelet analysis. In addition, climate change disrupts the stationarity and regularity of events previously regarded as periodic, with extreme floods, dry spells and droughts becoming more frequent (Cunha et al., 2019).

Regular wavelet analysis makes use of the convolution of a function (the "mother" wavelet) along the time series, in a moving window (Torrence & Compo, 1998). The convolution is repeated using stretched and shrunk versions of the mother wavelet. Significant frequencies, or harmonics, present in the time series are identified if their shape match that of the mother wavelet. Stretched versions of the mother wavelet result in higher convolution over lower frequencies, that is, longer peaks or oscillations; the convolution with shrunk versions identify higher frequencies, or short-lived peaks. The final result is the wavelet power, which can be visualized in a bi-dimensional plot with time on the *x*-axis and frequencies in the *y*-axis. Mathematically, the wavelet transform *W(t,a)* has units of the series variance as it is defined as:

$$W(t,a) = \frac{1}{\sqrt{a}} \int_{-\infty}^{\infty} x(\tau)\, \Psi^{*}\left(\frac{\tau - t}{a}\right) d\tau \quad (2)$$

where x is a time series, t is the time, τ is the integration variable along time, and a is the parameter that stretches and shrinks the mother wavelet Ψ (* denotes the complex conjugate). Mother wavelets should have zero mean and be localized in time, among other criteria. The most used functions are the Morlet, the Mexican hat, or the Haar (Jiang et al., 2006; Lovejoy & Schertzer, 2012; Mi et al., 2005; Torrence & Compo, 1998). In this study, the Morlet function was used since it was reported in previous works to be appropriate to identify features in geophysical time series (Liu et al., 2020; Sá et al., 1998; Zeri et al., 2019). The function is defined as:

$$\Psi(\eta) = \pi^{-1/4} \; e^{i\omega_0\eta} e^{-\eta^2/2} \tag{3}$$

where η and ω_0 are non-dimensional parameters of time and frequency, respectively, and i is the imaginary unit.

Cross-wavelet analysis is a variation of the technique that quantifies the variability of the covariance between two signals in time and frequency (Grinsted et al., 2004). The resulting cross-wavelet power $W_{xy}(t,a)$ has units of the covariance between signals x and y. The complex part of $W_{xy}(t,a)$ has information on the phase difference between x and y, which can be converted to temporal lags according to the following expression:

$$\lambda = T\left(\frac{\theta}{360}\right) \tag{4}$$

where λ is the temporal lag, in months, T is the time scale, in months, and θ is the phase angle, in degrees. The phase angle reference (zero degrees) is north, increasing in clockwise direction. Thus, East pointing arrows (90°) on the time scale of 12 months would results in a lag of 3 months. Cross-wavelet analysis was used in this work to investigate the temporal relationships between time series of climate indices such as the SMA, SPI, and VHI.

All calculations were made using Python 3.9 and the python package PyCWT (https://pypi.org/project/pycwt/), which has implementations of the original scripts for wavelet and cross-wavelet analysis (Grinsted et al., 2004; Torrence & Compo, 1998).

3 | RESULTS AND DISCUSSION

3.1 | Jules model evaluation with in situ data

Model and measurements of soil moisture were correlated over the region by comparing data from stations with the nearest grid points. The focus of the comparison was to evaluate the variability and trends of both datasets rather than aiming at precise absolute values of soil moisture. Nevertheless, the median correlation was approximately 0.48 over the domain, with median Root Mean Square Error (RMSE) and Mean Bias Error (MBE) of approximately 0.07 $m^3\ m^{-3}$ and 0.12 $m^3\ m^{-3}$, respectively (Figure 2). Spearman correlation coefficient was used for its robustness, since no assumption is made about the data having a normal distribution (which is assumed in Pearson correlation). In this figure, only stations where the correlation was statistically significant (at 5% level) were used, which resulted in the selection of 336 out of 360 stations (the bias of selecting only statistically significant correlations was negligible; the analysis considering all 360 stations resulted in a median correlation coefficient of 0.47).

Correlation varied among the domain according to soil texture classes. The three most common classes were loamy sand, sandy clay loam, and sandy loam, according to classes defined by the United States Department of Agriculture (USDA). Each one of those classes were observed over approximately 80 stations, accounting to 71% of the total; for those classes, median correlation between model and measured soil moisture was of 0.51 ± 0.15. What is common to those three classes is the sand content higher than 50% of the sample mass, which is consistent with the typical sandy soils observed over the Brazilian semiarid (Marques et al., 2014). Other significant texture classes were sand and clay, corresponding to 40 (12%) and 25 (7%) stations, respectively. Median correlation for those classes was of 0.50 ± 0.15 (sand) and 0.35 ± 0.15 (clay). Maximum correlation was 0.67 ± 0.15 for three stations with silty loam soil texture class.

Correlations of 0.6 to 0.7 between measurements and modelled estimates were reported before in a study using data from 12 networks over 4 continents (Albergel et al., 2012). However, measurements at several depths up to 1 m were used in that study, in addition to model estimates within a 3 m layer. The results in the current study between JULES surface soil moisture and in situ observations were considered satisfactory, especially as the model and measurements are not perfectly matched in terms of spatial scale and soil depth. The model data resulted in a good performance when considering identification of drought events and trends, as discussed below.

3.2 | Standardized soil moisture anomaly

Examples of SMA can be seen in Figure 3 for grid points next to three stations in the states of Rio Grande do Norte (north), Bahia (Centre), and Minas Gerais (south). Classes of ENSO were also included in this figure. The exact location of the three sites can be seen in Figure 4. The lowest values of SMA in the period were registered in 1983, 1994,

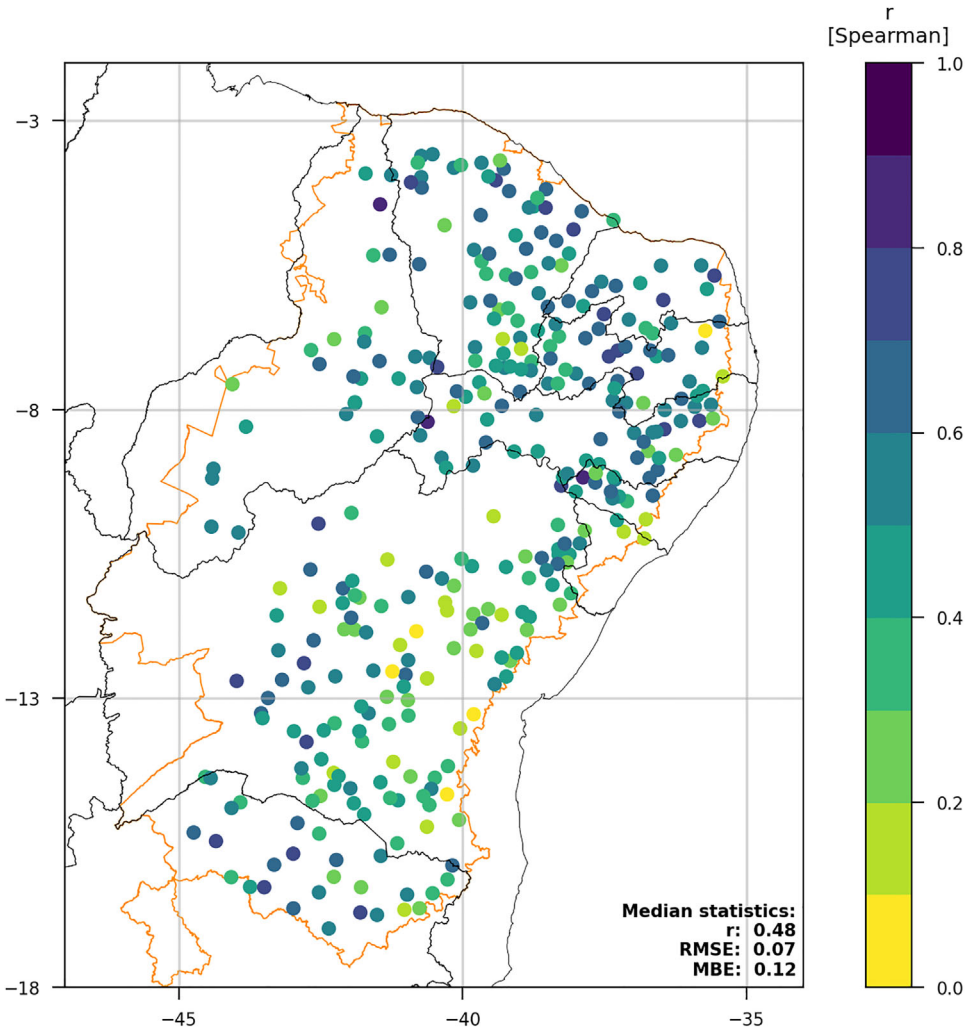

FIGURE 2 Correlation coefficient (Spearman) between measured and modelled (JULES) soil moisture. Median statistics computed using data from 2015 to 2018. Abbreviations: MBE, mean bias error; RMSE, root mean square error.

and 2012–2013, with values well below -1, generally considered as the lower bound of a normal condition for a standardized anomaly. The first year (1983) was associated with a very strong ENSO (1982–1983), the second event followed a strong ENSO (1992–1993), while 2012–2013 was the start of a five-year drought in the region (Brito et al., 2017). The very strong ENSO of 1997–1998 was associated with SMA values below -1 in all three locations. It is also evident that drought events which are strong in a region have a different magnitude in another, such as the period 2012–2013 which was associated with strong droughts in Rio Grande do Norte (panel a) but less intense events in the other two sites. Similarly, the El Niño of 1983, one of the strongest in the record, had a larger impact on the station of Minas Gerais (panel c), in comparison with the other two locations. Finally, the centre and south locations had SMI < -2 during the very strong ENSO of 2015–2016.

The different spatial patterns of drought according to SMA can be seen in Figure 4 (the colour scale), in addition to the growing season periods, and municipalities affected by drought. Three months were chosen to represent droughts: April 2012, April 2013, and January 2015. January and April are part of three rainy periods considered for agriculture in the Brazilian semiarid. The growing season periods which include the respective month are also shown in each panel of Figure 4. These periods were defined in a previous study that evaluated the start of the rainy season in the region (Brito et al., 2017). The drought in 2012 affected most of the Brazilian semiarid, covering all its latitudinal transect. Droughts were also registered in the following year (April 2013), and January 2015 was characterized by a strong drought in the south.

Rainfall in 2012, 2013 and 2015 was below the historical average within the Brazilian semiarid and contributed to drier soils and drought impacts. We considered the period from November to July since it includes all the rainy periods over the region. We sampled the CHIRPS database using the Jules model grid points (Figure 1c). Only the

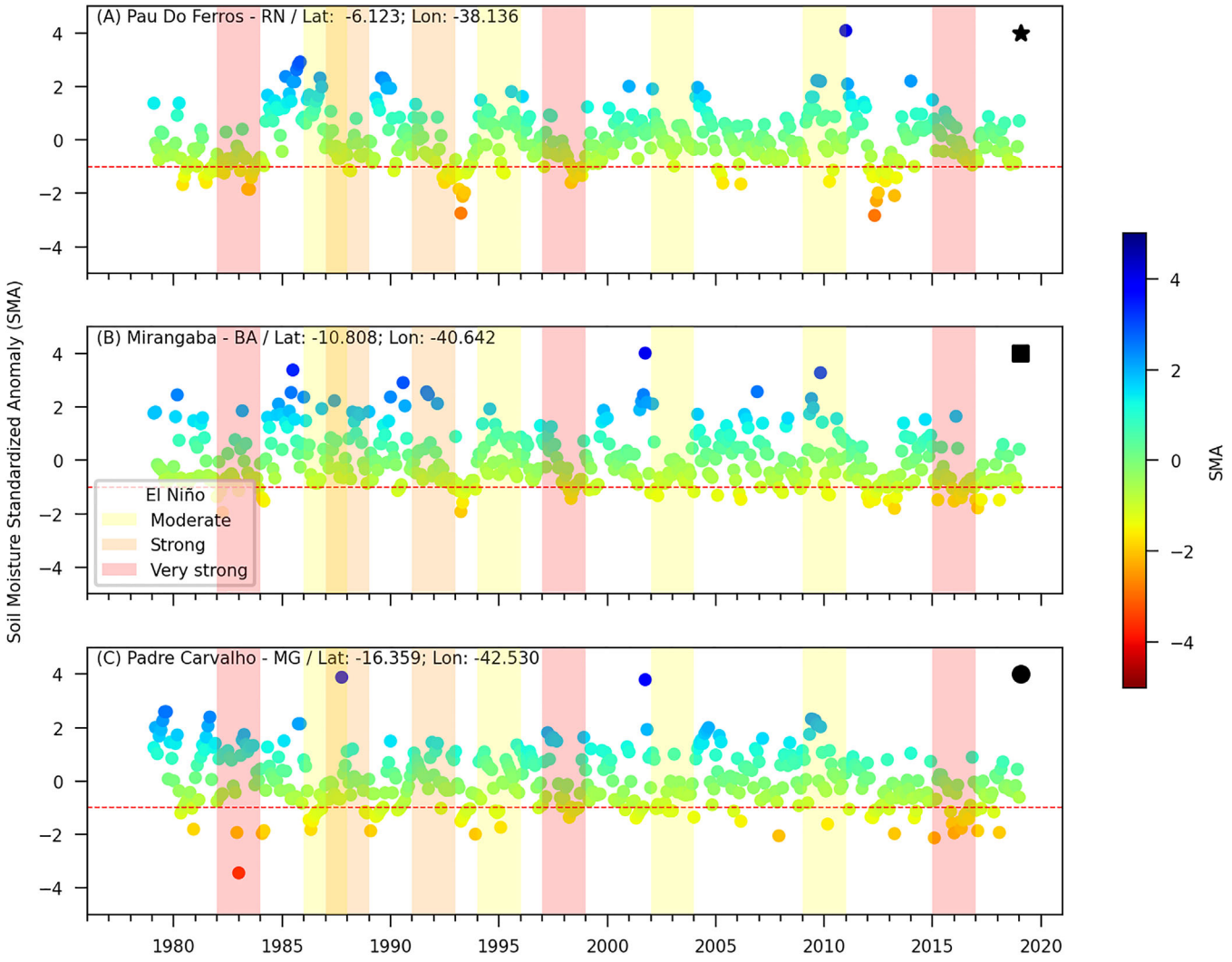

FIGURE 3 Time series of the Standardized Soil Moisture Index (SMA) for grid points over the north (top panel), centre (middle) and south (bottom) of the region. The horizontal line marks the value of −1, generally considered as the lower bound of a normal condition. The color scale is the same as *y*-axis values of SMA. The black symbols denote the locations similarly marked in Figure 4. ENSO classes based on the Oceanic Niño Index (ONI)

grid points within the semiarid were included. The mean cumulative rainfall from November to July, in the period of 1981 to 2020, was of 698 mm. Considering the same date range, the sum for 2011–2012, 2012–2013, and 2014–2015 was of 400, 553, and 653 mm, respectively.

The droughts in Figure 4 led to crop yield losses for rainfed agriculture, the predominant system in the region. The impacts of droughts on the region were assessed using data from the "Garantia Safra" program. Municipalities with verified droughts and yield losses are denoted with the red markers in Figure 4. Overall, the number of municipalities supported by the program during the cropping seasons of 2011–2012, 2012–2013, and 2014–2015 were, respectively 1015, 240, and 1014; these numbers correspond to 80.4%, 19.0%, and 80.3% of the 1262 municipalities which are located within the official Brazilian semiarid delimitation.

A negative anomaly in soil moisture leads to crop losses due to water stress and reduction in evapotranspiration. Some periods during the growing season are critical, such as the first 2 months after planting, in the case of maize, when vegetative growth and flowering stages occur. The number of drought events identified by SMA during the growing season was counted and compared with events identified by SPI (Figure 5). The criterion used was based on values of SMA lower than -1 in the first or second months of the growing season. The same approach was used for SPI. The search was made for each of the model grid points. The growing season at each of the grid points is illustrated in Figure 5a. Grid points were selected by the intersection with the rainy season (growing season) contours in Figure 4. The results in Figure 5b show that on average 5 to 12 drought events were recorded by SMA or

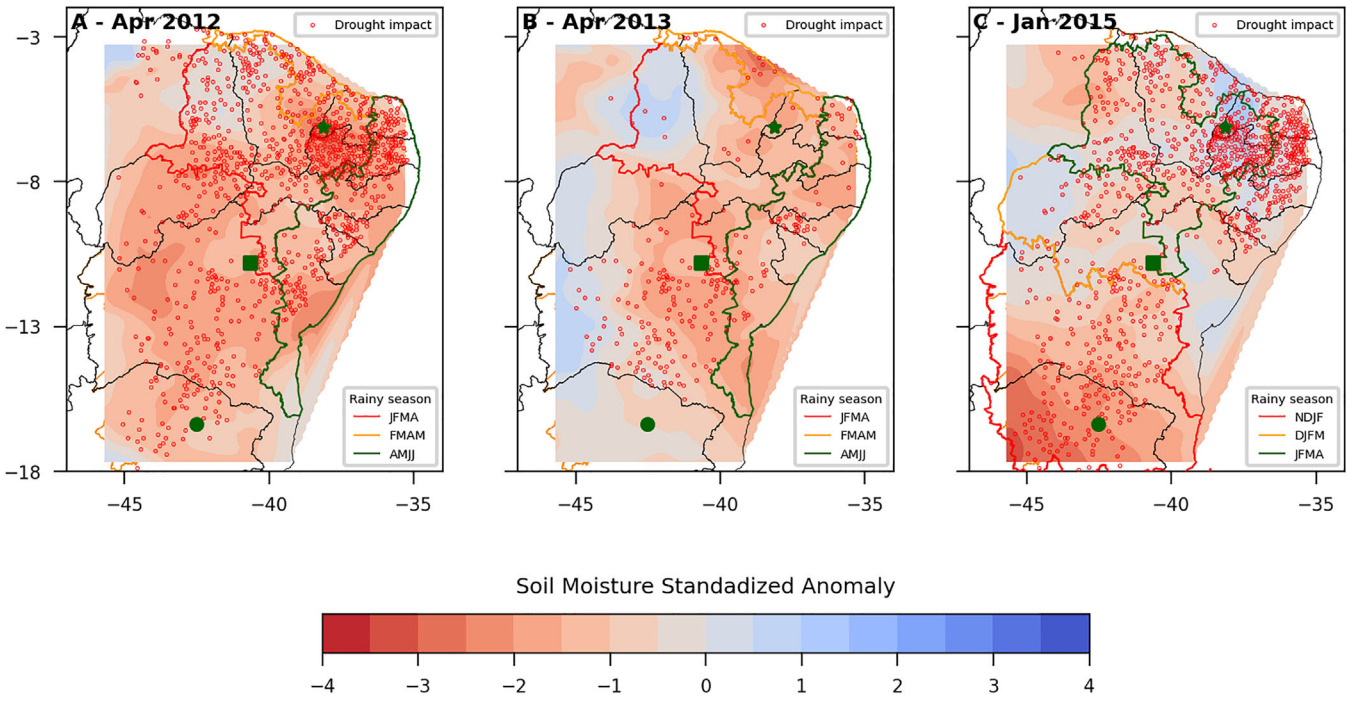

FIGURE 4 Standardized Soil Moisture Index interpolated over the region for (a) April 2012, (b) April 2013 and (c) January 2015. Symbols ★, ■, and • denote the locations in top, middle and bottom panels of Figure 3, respectively. Red markers denote municipalities with verified drought impact, according to the "Garantia Safra" crop insurance program. The contour lines mark the rainy periods associated with the month shown in the figure

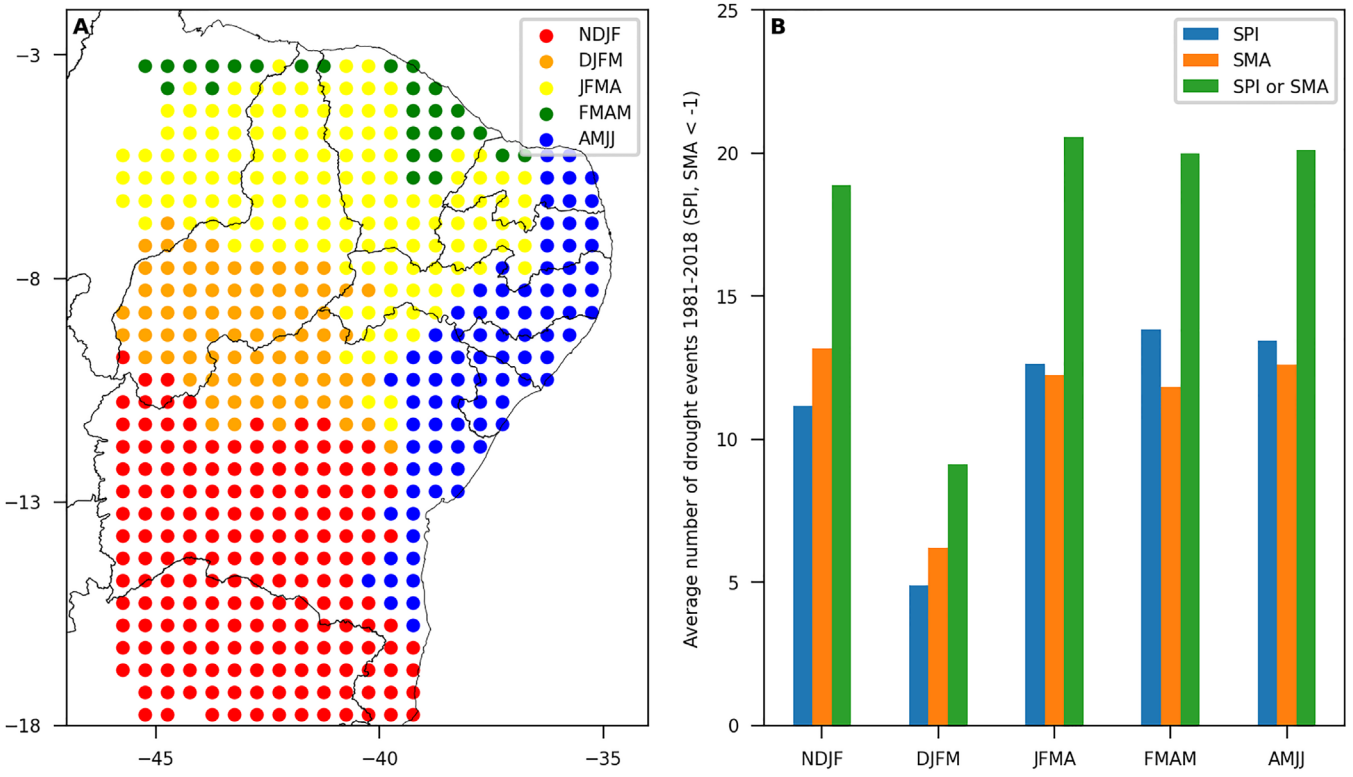

FIGURE 5 (a) Grid points coloured according to the rainy period; (b) Average number of drought events during the first 2 months of the rainy period according to SPI, SMA, and SPI or SMA. Period of analysis: 1981–2019

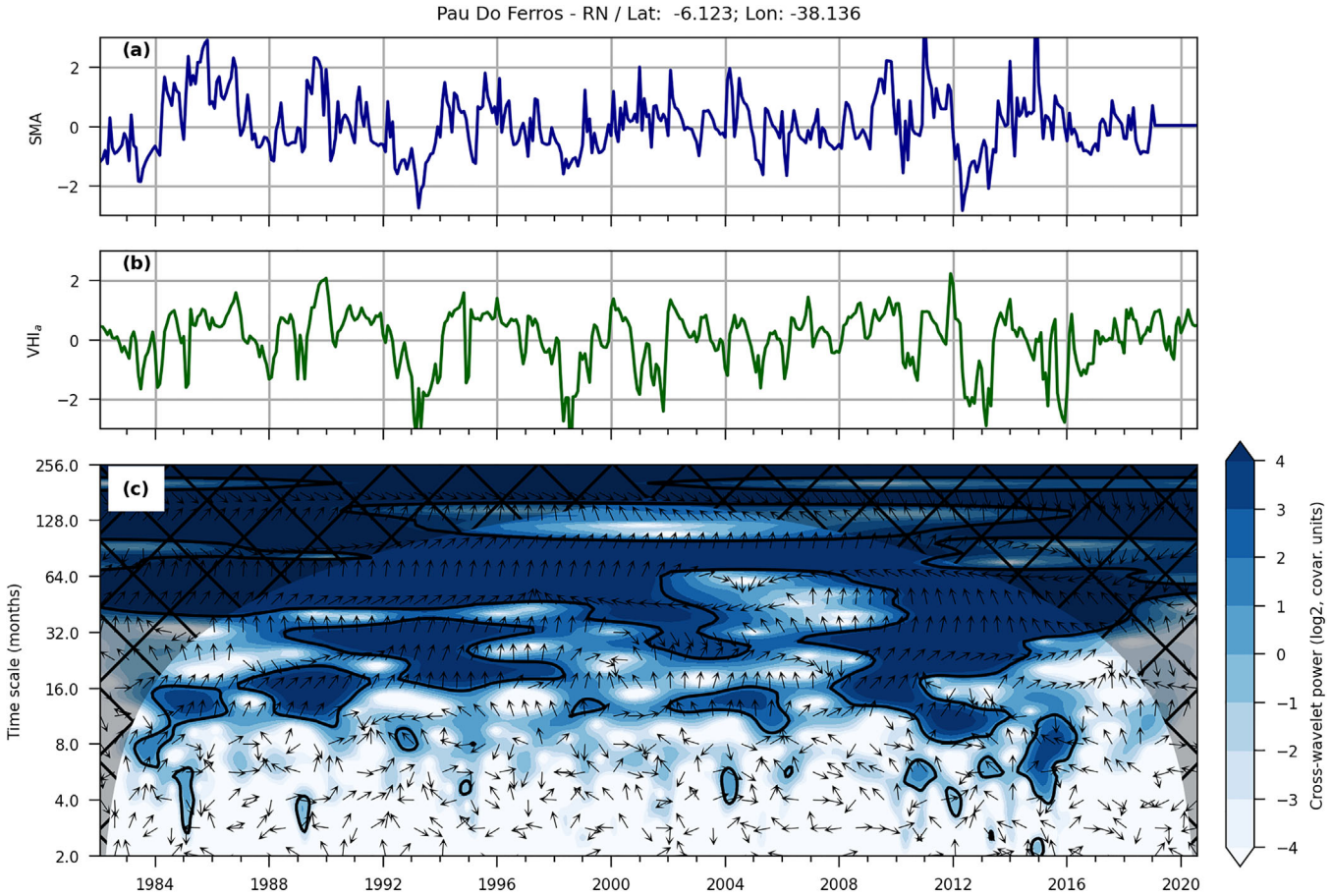

FIGURE 6 (a) Time series of SMA next to the location marked with ★ in Figure 4; (b) VHI anomaly at the same location; (c) cross-wavelet power between SMA and VHI_a. Black contours denote areas statistically significant; the shaded area is not considered due to the influence of the series edges; arrows denote the phase difference between signals in the corresponding time scale (*y*-axis). Location coordinates: −6.123 (latitude), −38.136 (longitude).

SPI, independently (blue and orange bars). The region of rainy period in DJFM was the one with the lowest number of events. Typically, both indices differ by 1 or 2 events identified. When both SPI and SMA criteria are combined (green bar), the number of drought events reaches approximately 20 in 4 of the 5 classes, suggesting that both indices are complementary in identifying drought. Drought events identified by SMA and SPI simultaneously (not shown) accounted for approximately half of each individual score (5/6 events in JFMA class, for example). Thus, double accounting is expected in the green bar in Figure 5b, especially because rainfall and soil moisture are strongly correlated. However, this redundancy is irrelevant when the main objective is an assessment of drought with complementary indices. This result shows that an integrated index that considers SMA and SPI, among other indices and indicators, might more suitable to identify drought due to the different temporal and spatial scales identified by individual components, such as rainfall, soil moisture, and vegetation status.

3.3 | Cross-wavelet analysis

The impacts of SMA on drought detection in the region was assessed using cross-wavelet analysis. This technique enables the calculation of correlation between two time series taking into account lagged relationships. This is especially useful to assess the impact of soil moisture deficit due to the delay in plants to respond to water stress in the soil (Adegoke &Carleton, 2002). The cross wavelet between SMA and VHI anomaly (VHI_a) was applied for the same sites shown in Figure 3 (in Figures 6, 7, and 8, respectively).

Significant cross wavelet power (within the closed contours) between SMA and VHI_a are found ranging from 2 to 128 months, during the whole period. However, the significant contributions on a given time scale, such as 16 months, are intermittent. Overall, the strongest cross wavelet power is found between 8 and 64 months, denoting strong covariance between SMA and VHI_a with annual to interannual variability. Most of the arrows inside the closed contours

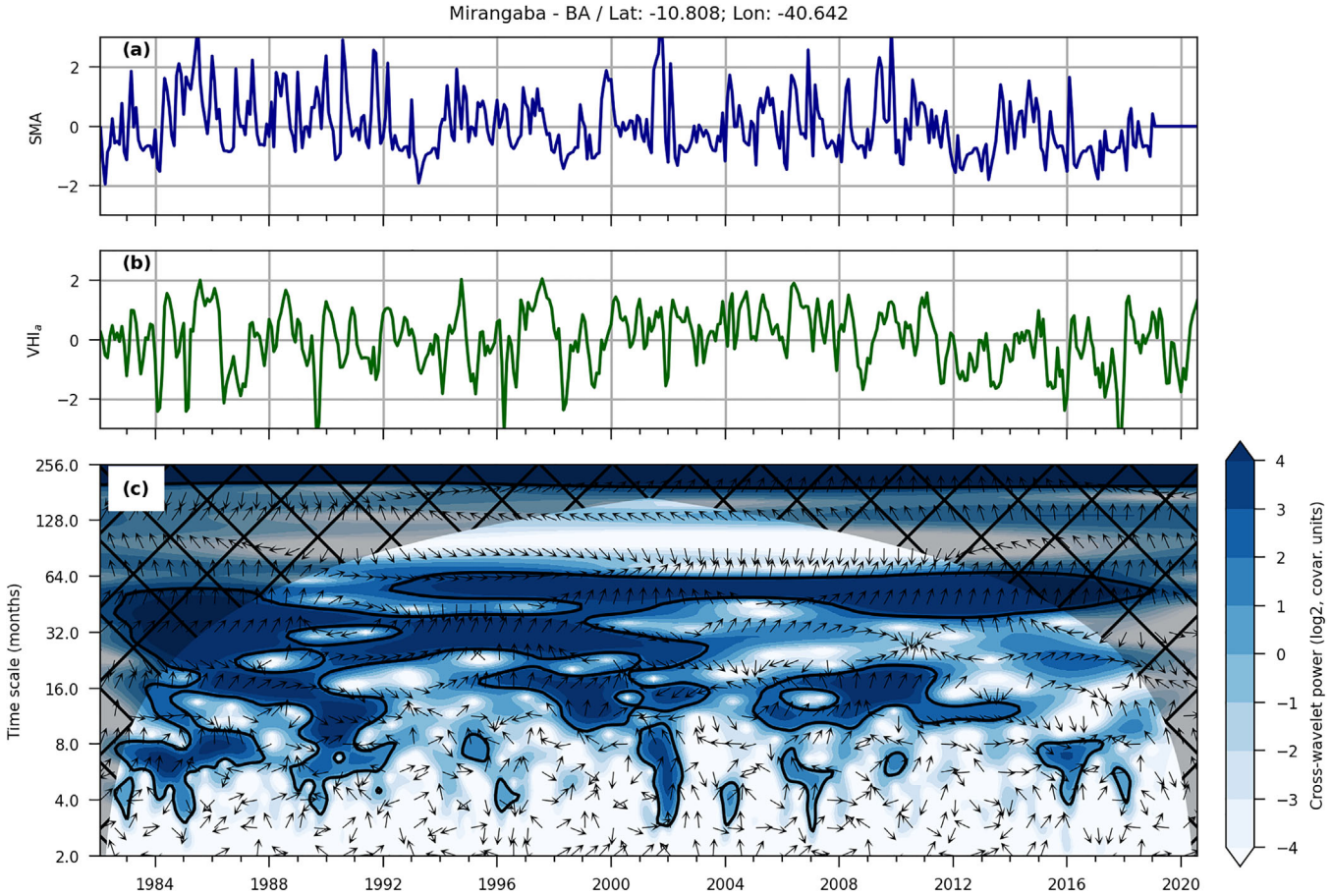

FIGURE 7 Similar to Figure 6, for the location marked with ■ in Figure 4. Location coordinates: −10.808 (latitude), −40.642 (longitude)

have 0–45° angles, approximately. In the annual time scale (12 months) angles are mostly 30–45°, especially from 1984 to 1992, and 2008 to 2014 (Figures 6 and 7). The angles of 30 to 45° would result in lags of VHI_a in relation to SMA on the order of 1 to 1.5 months in the annual time scale. Thus, variability in SMA could be used as an early warning to anomalies in VHI_a. A strong negative anomaly of SMA in the first month after planting indicate likely impacts on crop growth, as indicated by VHI_a. Negative anomalies after the crop development and flowering stages, such as 30 to 60 days after planting for maize, could result in impacts on final yields expected on the following month.

Interannual variability is also evident in the cross-wavelet analysis between SMA and VHI_a, especially around 32 to 64 months (approximately 3 to 5 years). In Figure 6, negative anomalies of SMA and VHI_a were correlated from 1992 to 1994, around 1998, and from 2012 to 2014. The arrows in the time scale of 64 months are mostly upwards (zero angle), indicating negligible lag. The first two events were associated with ENSO. The interannual variability observed in Figure 6 is not the same observed in Figures 7 and 8 due to the different susceptibility to interannual variability in the corresponding locations. Historically, the northern part of the Brazilian semiarid region is strongly associated drought caused by ENSO variability (Hastenrath & Heller, 1977; Hastenrath, 2006; Pezzi & Cavalcanti, 2001; Tomasella et al., 2018). Two patterns are evident in Figure 8: (1) almost no significant cross wavelet power exists after 2008 from time scales up to 32 months; (2) strong interannual variability of 20 years (1996 to 2016). The second pattern cannot be resolved by this analysis due to the series length, since the 20 years' time scale (240 months) falls within the "cone of influence", the shaded and hatched area where results are affected by time series edge effects.

To check whether SMA and SPI have similar performance in terms of temporal variability with VHI_a, cross-wavelet analysis was applied to the relationship between SPI and VHI_a (Figure S2, Supporting Information, for the Pau dos Ferros, RN, site). Overall, the relationship between SPI and VHI_a is similar to the one observed for SMA and VHI_a especially due to the significant time scales in the range of 4 to 64 months; and the average lag between series around 30–45°. The agreement between SMA and SPI at this location can be seen in the cross wavelet in Figure S3, Supporting Information. The arrows within the

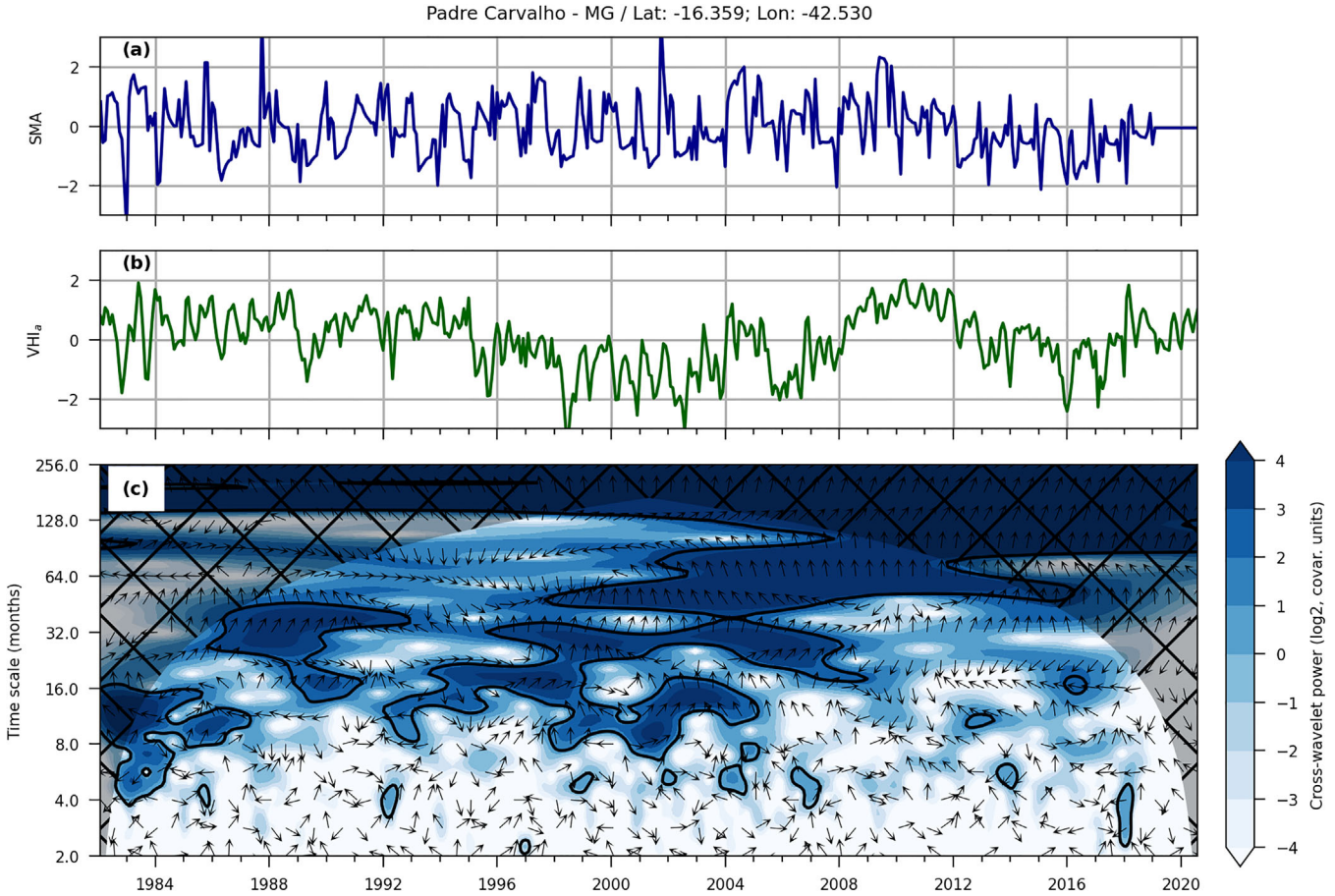

FIGURE 8 Similar to Figure 6, for the location marked with • in Figure 4. Location coordinates: −16.359 (latitude), −42.530 (longitude)

contour lines are mostly vertical, with small angles in some cases, indicating small temporal lags. According to the rainy quarters of Figure 4, the *Pau dos Ferros* site (star) is located within the JFMA limits. In fact, the average number of drought events for the JFMA in Figure 5 was approximately 12 for both SMA and SPI.

The same analysis was done for the other sites over the middle and south of the domain comparing cross wavelets between SPI and VHI_a, and SMA and SPI (results not shown). For the Bahia site (middle), more events were significant in the SPI x VHI_a cross wavelet in comparison with SMA × VHI_a (Figure 7) especially after 2016 in the annual time scale. For the southern site, the significant cross wavelet power events between SPI and VHI_a were sparser in time, short-lived, and absent above the time scale of 32 months, in comparison with results in Figure 8. This site was also the one with the highest number of significant events between SPI and SMA in the time scale of 4 months (in relation to Figure S3, Supporting Information).

Intra-annual variability was observed in time scales from 2 to 8 months in Figures 6–8, and in Figures S2 and S3, Supporting Information. In this case, the analysis of phase relationships and lags in time is not conclusive due to the short nature of events. However, a significant event can be seen in 2016 around time scale of 4–8 months (Figure 7). In this case, arrows are almost horizontal at 90°, indicating a VHI_a lag of ¼ of the time scale, or 1–2 months, in relation to SMA. Other significant event with similar characteristics of time scale and lag was found in the relationship between SPI and VHI_a for the same site (not shown).

Overall, SMA and SPI have similarities and differences when used to identify droughts, in agreement in the accounting of events in Figure 5. The differences across the latitudinal extent are expected due to several reasons, namely: (1) different climate and weather patterns; (2) differences in soil characteristics and desertification; and (3) different biomes. The northern part of the Brazilian semiarid is affected by climate teleconnections with the Pacific and Atlantic Oceans. This influence is weaker as one moves southwards. Soils over the Brazilian semiarid are mostly sandy, but the proportion of clay content is higher over the southern part of the domain (Zeri et al., 2018). Soils with high clay content hold more water, which can affect the dynamics of soil moisture and evaporation. Finally, the southern part of the Brazilian semiarid has three biomes (Figure 1): *Caatinga*, *Cerrado* and Atlantic Forest. Different

kinds of vegetation affect the water cycle and relationships between rainfall, soil moisture, and evapotranspiration.

The results presented here show a good performance of the JULES soil moisture when applied to identify the spatial and temporal relationships (or patterns) of droughts in the Brazilian semiarid. These findings highlight the importance of using datasets from different sources (model outputs, remote sensing, in situ information), such as rainfall anomalies, soil moisture deficit, and vegetation indices to reduce the uncertainty of drought assessments. Long-term datasets of *in-situ* soil moisture data are scarce, especially over the Brazilian semiarid region. The use of hydrological or land surface models can fill this gap by providing long-term outputs and enabling the calculation of anomalies and trends. Future studies should focus on testing of different models and combination with other indices.

4 | CONCLUSIONS

Soil moisture is essential to crop growth and development and its deficit on short and long terms can lead to impacts on rainfed and subsistence agriculture. Long-term time-series of soil moisture measurements are rarely available in most parts of the world. Modelling of the water balance is an alternative to obtain time series of soil moisture, enabling the identification of trends and characterization of droughts especially agricultural droughts.

Drought monitoring usually makes use of rainfall deficits over different temporal scales. Recent approaches make use of rainfall, soil moisture and vegetation indices to assess drought in a combined way, integrating different temporal and spatial scales. The results presented in this work show that the soil moisture from the JULES land surface model correctly identifies drought events over the Brazilian semiarid. The model outputs were used to calculate an anomaly of soil moisture which responds to droughts over the region. The resulting index has a good performance identifying drought events when compared to SPI. The index SMA is also well correlated with VHI, indicating that negative anomalies in soil moisture led to impacts on plant development. Future studies should be carried out with the objective of testing additional models for the soil water over the region, in combination with different drought indices and indicators.

An important step to improve drought monitoring is the development of significant technical capacity in terms of information database, which is reflected in reliable early warning systems aiming at reducing vulnerability of people at risk (Gutiérrez et al., 2014; Wilhite et al., 2014). In this sense, the results presented in this paper support the conclusion that an integrated approach with anomalies of soil moisture, rainfall and vegetation indices should be preferred when designing a monitoring system in order to capture different aspects of drought. Drought monitoring and assessment should make use of different tools to identify spatial and temporal patterns. The use of soil moisture from hydrological or land surface models, and satellite products is an alternative to complement the current tools such as SPI and vegetation indices. Drought management policy for Brazil, especially over the semiarid region, should make use of all available sources of information in an integrated way.

ACKNOWLEDGEMENTS

Eleanor M. Blyth, Garry D. Hayman, Murilo S. Vianna, Marcelo V. Galdos, Karina Williams, and Toby R. Marthews acknowledge the support of the Newton Fund, through the UK Met Office administered programme "Climate Science for Service Partnership Brazil" (CSSP Brazil) and the CSSP Brazil project "Developing impacts modelling capability and understanding—Agricultural crop modelling and application" (grant DN373701). Gisleine Cunha-Zeri is grateful to Coordination for the Improvement of Higher Education Personnel (CAPES)—grant 88887.308408/2018-00.

REFERENCES

Adegoke, J.O. & Carleton, A.M. (2002) Relations between soil moisture and satellite vegetation indices in the U.S. Corn Belt. *Journal of Hydrometeorology*, 3, 395–405. Available from: https://doi.org/10.1175/1525-7541(2002)003⟨0395:RBSMAS⟩2.0.CO;2

Alam, M., Emura, K., Farnham, C. & Yuan, J. (2018) Best-fit probability distributions and return periods for maximum monthly rainfall in Bangladesh. *Climate*, 6, 9. Available from: https://doi.org/10.3390/cli6010009

Albergel, C., de Rosnay, P., Balsamo, G., Isaksen, L. & Muñoz-Sabater, J. (2012) Soil moisture analyses at ECMWF: Evaluation using global ground-based in situ observations. *Journal of Hydrometeorology*, 13(5), 1442–1460. Available from: https://doi.org/10.1175/JHM-D-11-0107.1

Alvalá, R.C.S., Cunha, A.P.M.A., Brito, S.S.B., Seluchi, M.E., Marengo, J.A., Moraes, O.L.L., et al. (2019) Drought monitoring in the Brazilian semiarid region. *Anais da Academia Brasileira de Ciências*, 91. Available from: https://doi.org/10.1590/0001-3765201720170209

Alves, F. (2009) O Programa Garantia-Safra no Semiárido Brasileiro. In: Cardoso, J.C., Gusso, D.A., Araujo, H.E., Chaves, J.V., Tironi, L.F., Azevedo, L.C.L., Aquino, L.M.C., Cassiolato, M.M.M.C., Lobo, M., Castro, P.R.F., & Davison, P.M.A. (Eds.) *Brasil Em Desenvolvimento—Estado, Planejamento e Políticas Publicas*. Brasilia, Brazil: Instituto de Pesquisa Econômica Aplicada (IPEA), p. 312.

Best, M.J., Pryor, M., Clark, D.B., Rooney, G.G., Essery, R.L.H., Ménard, C.B., et al. (2011) The Joint UK Land Environment Simulator (JULES), model description—Part 1: Energy and water fluxes. *Geoscientific Model Development*, 4, 677–699. Available from: https://doi.org/10.5194/gmd-4-677-2011

Bett, P.E., Williams, K.E., Burton, C., Scaife, A.A., Wiltshire, A.J. & Gilham, R. (2020) Skillful seasonal prediction of key carbon cycle components: NPP and fire risk. *Environmental Research Communications*, 2, 055002. Available from: https://doi.org/10.1088/2515-7620/ab8b29

Blyth, E., Clark, D.B., Ellis, R., Huntingford, C., Los, S., Pryor, M., et al. (2011) A comprehensive set of benchmark tests for a land surface model of simultaneous fluxes of water and carbon at both the global and seasonal scale. *Geoscientific Model Development*, 4(2), 255–269. Available from: https://doi.org/10.5194/gmd-4-255-2011

Bokusheva, R., Kogan, F., Vitkovskaya, I., Conradt, S. & Batyrbayeva, M. (2016) Satellite-based vegetation health indices as a criteria for insuring against drought-related yield losses. *Agricultural and Forest Meteorology*, 220, 200–206. Available from: https://doi.org/10.1016/j.agrformet.2015.12.066

Brito, S.S.B., Cunha, A.P.M.A., Cunningham, C.C., Alvalá, R.C., Marengo, J.A. & Carvalho, M.A. (2017) Frequency, duration and severity of drought in the semiarid northeast Brazil region. *International Journal of Climatology*, 38, 517–529. Available from: https://doi.org/10.1002/joc.5225

Cammalleri, C., Micale, F. & Vogt, J. (2015) On the value of combining different modelled soil moisture products for European drought monitoring. *Journal of Hydrology*, 525, 547–558. Available from: https://doi.org/10.1016/j.jhydrol.2015.04.021

Cao, Y., Chen, S., Wang, L., Zhu, B., Lu, T. & Yu, Y. (2019) An agricultural drought index for assessing droughts using a water balance method: A case study in Jilin Province, Northeast China. *Remote Sensing*, 11, 1066. Available from: https://doi.org/10.3390/rs11091066

Carrão, H., Russo, S., Sepulcre-Canto, G. & Barbosa, P. (2016) An empirical standardized soil moisture index for agricultural drought assessment from remotely sensed data. *International Journal of Applied Earth Observation and Geoinformation*, 48, 74–84. Available from: https://doi.org/10.1016/j.jag.2015.06.011

Cavalcante, R.B.L., Ferreira, D.B.S., Pontes, P.R.M., Tedeschi, R.G., da Costa, C.P.W. & de Souza, E.B. (2020) Evaluation of extreme rainfall indices from CHIRPS precipitation estimates over the Brazilian Amazonia. *Atmospheric Research*, 238, 104879. Available from: https://doi.org/10.1016/j.atmosres.2020.104879

Cavalcanti, A.S. (2009) *Avaliações de padrões atmosféricos associados à ocorrência de chuvas extremas no litoral da região Nordeste do Brasil: Aspectos numéricos na previsão operacional do tempo*. Rio de Janeiro, Brazil: COPPE/UFRJ. COPPE/Universidade Federal do Rio de Janeiro.

Clark, D.B., Mercado, L.M., Sitch, S., Jones, C.D., Gedney, N., Best, M.J., et al. (2011) The Joint UK Land Environment Simulator (JULES), model description—Part 2: Carbon fluxes and vegetation dynamics. *Geoscientific Model Development*, 4, 701–722. Available from: https://doi.org/10.5194/gmd-4-701-2011

Collatz, G., Ribas-Carbo, M. & Berry, J. (1992) Coupled photosynthesis-stomatal conductance model for leaves of C4 plants. *Functional Plant Biology*, 19, 519–538. Available from: https://doi.org/10.1071/PP9920519

Collatz, G.J., Ball, J.T., Grivet, C. & Berry, J.A. (1991) Physiological and environmental regulation of stomatal conductance, photosynthesis and transpiration: A model that includes a laminar boundary layer. *Agricultural and Forest Meteorology*, 54, 107–136. Available from: https://doi.org/10.1016/0168-1923(91)90002-8

Cunha, A.P.M., Alvalá, R.C., Nobre, C.A. & Carvalho, M.A. (2015) Monitoring vegetative drought dynamics in the Brazilian semiarid region. *Agricultural and Forest Meteorology*, 214–215, 494–505. Available from: https://doi.org/10.1016/j.agrformet.2015.09.010

Cunha, A.P.M.A., Tomasella, J., Ribeiro-Neto, G.G., Brown, M., Garcia, S.R., Brito, S.B., et al. (2018) Changes in the spatial–temporal patterns of droughts in the Brazilian Northeast. *Atmospheric Science Letters*, 19, e855. Available from: https://doi.org/10.1002/asl.855

Cunha, A.P.M.A., Zeri, M., Deusdará Leal, K., Costa, L., Cuartas, L.A., Marengo, J.A., et al. (2019) Extreme drought events over Brazil from 2011 to 2019. *Atmosphere*, 10, 642. Available from: https://doi.org/10.3390/atmos10110642

De Alcântara Silva, V.M., Marcelino Patrício, M.C., Ribeiro, V.H.A. & Mainar De Medeiros, R. (2013) O desastre seca no nordeste brasileiro. *POLÊM!CA* 12(2), 284–293.

de Souza, E.B., Kayano, M.T. & Ambrizzi, T. (2005) Intraseasonal and submonthly variability over the Eastern Amazon and Northeast Brazil during the autumn rainy season. *Theoretical and Applied Climatology*, 81, 177–191. Available from: https://doi.org/10.1007/s00704-004-0081-4

Dijkshoorn, J.A., Huting, J.R.M. & Tempel, P. (2005) Update of the 1:5 million Soil and Terrain Database for Latin America and the Caribbean (SOTERLAC; version 2.0), ISRIC. Report 2005/01.

Ellis, R.J., Taylor, C.M., Weedon, G.P., Gedney, N., Clark, D.B. & Los, S. (2009) Evaluating the simulated seasonality of soil moisture with earth observation data. *Journal of Hydrometeorology*, 10, 1548–1560. Available from: https://doi.org/10.1175/2009JHM1147.1

FAO (2017) *The future of food and agriculture: Trends and challenges*. Rome: Food and Agriculture Organization of the United Nations.

Farinelli, B., Valdivia, P. & Arias, D. (2017) Municipal agricultural drought preparedness and response plan. In: Nys, E., Engle, N.L., Magalhães, A.R. (Eds.) *Drought in Brazil: Proactive management and policy*. Boca Raton, FL: Taylor & Francis Group, pp. 67–80.

Funk, C.C., Peterson, P.J., Landsfeld, M.F., Pedreros, D.H., Verdin, J.P., Rowland, J.D., et al. (2014) A quasi-global precipitation time series for drought monitoring. *U.S. Geological Survey Data Series 832*.

Godfray, H.C.J., Beddington, J.R., Crute, I.R., Haddad, L., Lawrence, D., Muir, J.F., et al. (2010) Food security: The challenge of feeding 9 billion people. *Science*, 327, 812–818. Available from: https://doi.org/10.1126/science.1185383

Gonçalves, G.R. (2000) *As secas na Bahia do século XIX. Faculdade de Filosofia e Ciências Humanas*. Salvador, Brasil: Universidade Federal da Bahia.

Grinsted, A., Moore, J.C. & Jevrejeva, S. (2004) Application of the cross wavelet transform and wavelet coherence to geophysical time series. *Nonlinear Processes in Geophysics*, 11, 561–566. Available from: https://doi.org/10.5194/npg-11-561-2004

Gutiérrez, A.P.A., Engle, N.L., de Nys, E., Molejón, C. & Martins, E.S., (2014) Drought preparedness in Brazil. *Weather and Climate Extremes*, 3, 95–106. Available from: https://doi.org/10.1016/j.wace.2013.12.001

Haddeland, I., Clark, D.B., Franssen, W., Ludwig, F., Voß, F., Arnell, N.W., et al. (2011) Multimodel estimate of the global terrestrial water balance: Setup and first results. *Journal of Hydrometeorology*, 12, 869–884. Available from: https://doi.org/10.1175/2011JHM1324.1

Hansen, J., Hellin, J., Rosenstock, T., Fisher, E., Cairns, J., Stirling, C., et al. (2019) Climate risk management and rural poverty reduction. *Agricultural Systems*, 172, 28–46. Available from: https://doi.org/10.1016/j.agsy.2018.01.019

Hastenrath, S. (2006) Circulation and teleconnection mechanisms of northeast Brazil droughts. *Progress in Oceanography*, 70, 407–415. Available from: https://doi.org/10.1016/j.pocean.2005.07.004

Hastenrath, S. & Heller, L. (1977) Dynamics of climatic hazards in northeast Brazil. *Quarterly Journal of the Royal Meteorological Society*, 103, 77–92. Available from: https://doi.org/10.1002/qj.49710343505

Holmgren, M., Stapp, P., Dickman, C.R., Gracia, C., Graham, S., Gutiérrez, J.R., et al. (2006) Extreme climatic events shape arid and semiarid ecosystems. *Frontiers in Ecology and the Environment*, 4, 87–95. Available from: https://doi.org/10.1890/1540-9295(2006)004[0087:ECESAA]2.0.CO;2

IBGE (2019a) Censo demográfico. Instituto Brasileiro de Geografia e Estatística. Available at: www.ibge.gov.br

IBGE (2019b) Biomas e sistema costeiro-marinho do Brasil: compatível com a escala 1:250 000. Rio de Janeiro: Instituto Brasileiro de Geografia e Estatística.

Iwema, J., Rosolem, R., Rahman, M., Blyth, E. & Wagener, T. (2017) Land surface model performance using cosmic-ray and point-scale soil moisture measurements for calibration. *Hydrology and Earth System Sciences*, 21, 2843–2861. Available from: https://doi.org/10.5194/hess-21-2843-2017

Jiang, Z., Yu, Q., Wang, T., Sun, X. & Zhang, R. (2006) Continuous wavelet transform and discrete multi-resolution analysis of surface fluxes and atmospheric stability. *Progress in Natural Science: Materials International*, 16, 403–409. Available from: https://doi.org/10.1080/10020070612330011

Kogan, F. (2002) World droughts in the new millennium from AVHRR-based vegetation health indices. *Eos, Transactions American Geophysical Union*, 83, 557–563. Available from: https://doi.org/10.1029/2002EO000382

Kogan, F.N. (1995) Application of vegetation index and brightness temperature for drought detection. *Advances in Space Research*, 15, 91–100. Available from: https://doi.org/10.1016/0273-1177(95)00079-T

Kogan, F.N. (1997) Global drought watch from space. *Bulletin of the American Meteorological Society*, 78, 621–636. Available from: https://doi.org/10.1175/1520-0477(1997)078⟨0621:GDWFS⟩2.0.CO;2

Kousky, V.E. (1979) Frontal influences on northeast Brazil. *Monthly Weather Review*, 107, 1140–1153. Available from: https://doi.org/10.1175/1520-0493(1979)107<1140:FIONB>2.0.CO;2

Kühne, E. (2020) Building climate resilience through social protection in Brazil: The Garantia-Safra public climate risk insurance programme. Brasilia, Brazil: IPC-IG.

Lima, A.O., Lyra, G.B., Abreu, M.C., Oliveira-Júnior, J.F., Zeri, M. & Cunha-Zeri, G. (2021) Extreme rainfall events over Rio de Janeiro State, Brazil: Characterization using probability distribution functions and clustering analysis. *Atmospheric Research*, 247(105221), https://doi.org/10.1016/j.atmosres.2020.105221

Liu, D.L., Teng, J., Ji, F., Anwar, M.R., Feng, P., Wang, B., et al. (2020) Characterizing spatiotemporal rainfall changes in 1960–2019 for continental Australia. *International Journal of Climatology*, 41(Suppl. 1), E2420–E2444. https://doi.org/10.1002/joc.6855

Lovejoy, S. & Schertzer, D. (2012) Haar wavelets, fluctuations and structure functions: Convenient choices for geophysics. *Nonlinear Processes in Geophysics*, 19, 513–527. Available from: https://doi.org/10.5194/npg-19-513-2012

Lyra, G.B., Oliveira-Júnior, J.F., Gois, G., Cunha-Zeri, G. & Zeri, M. (2017) Rainfall variability over Alagoas under the influences of SST anomalies. *Meteorology and Atmospheric Physics*, 129, 157–171. Available from: https://doi.org/10.1007/s00703-016-0461-1

Magalhaes, A.R. (2017) Life and drought in Brazil. In: Nys, E., Eagle, N.L., Magalhaes, A.R. (Eds.) *Drought in Brazil: Proactive management and policy*. Boca Raton, FL: Taylor & Francis Group, pp. 1–18.

MAPA (2020) Garantia Safra. Ministério da Agricultura, Pecuária e Abastecimento. Available at: https://www.gov.br/agricultura/pt-br/assuntos/politica-agricola/garantia-safra [Accessed 2nd December 2020).

Marques, F.A., Nascimento, A.F., Araujo Filho, J.C. & Silva, A.B. (2014) Solos do nordeste. Available at: http://ainfo.cnptia.embrapa.br/digital/bitstream/item/114582/1/FOLDER-SOLOS-DO-NE-versao-final.pdf [Accessed 15th April 2021].

Marthews, T.R., Jones, R.G., Dadson, S.J., Otto, F.E.L., Mitchell, D., Guillod, B.P., et al. (2019) The impact of human-induced climate change on regional drought in the Horn of Africa. *Journal of Geophysical Research: Atmospheres*, 124, 4549–4566. Available from: https://doi.org/10.1029/2018JD030085

Marthews, T.R., Malhi, Y., Girardin, C.A.J., Silva Espejo, J.E., Aragão, L.E.O.C., Metcalfe, D.B., et al. (2012) Simulating forest productivity along a Neotropical elevational transect: Temperature variation and carbon use efficiency. *Global Change Biology*, 18. Available from: https://doi.org/10.1111/j.1365-2486.2012.02728.x

Martínez-de la Torre, A., Blyth, E. & Robinson, E. (2019) Evaluation of drydown processes in global land surface and hydrological models using flux tower evapotranspiration. *Water*, 11, 356. Available from: https://doi.org/10.3390/w11020356

McKee, T.B., Doesken, N.J. & Kleist, J. (1993) The relationship of drought frequency and duration to time scales. In: Proceedings of the 8th conference on applied climatology, Boston, MA, pp. 179–184.

McKee, T.B., Doesken, N.J. & Kleist, J. (1995) Drought monitoring with multiple time scales. In: Proceedings of the 9th conference on applied climatology, Dallas, TX, pp. 233–236.

Mi, X., Ren, H., Ouyang, Z., Wei, W. & Ma, K. (2005) The use of the Mexican Hat and the Morlet wavelets for detection of ecological patterns. *Plant Ecology*, 179, 1–19. Available from: https://doi.org/10.1007/s11258-004-5089-4

Milhorance, C., Sabourin, E., le Coq, J.-F. & Mendes, P. (2020) Unpacking the policy mix of adaptation to climate change in Brazil's semiarid region: Enabling instruments and coordination mechanisms. *Climate Policy*, 20(5), 593–608. https://doi.org/10.1080/14693062.2020.1753640

Mishra, A.K. & Singh, V.P. (2010) A review of drought concepts. *Journal of Hydrology*, 391, 202–216. Available from: https://doi.org/10.1016/j.jhydrol.2010.07.012

Nogueira, S.M.C., Moreira, M.A. & Volpato, M.M.L. (2018) Evaluating precipitation estimates from Eta, TRMM and CHRIPS data in the south-southeast region of Minas Gerais state-Brazil. *Remote Sensing*, 10(2), 313. Available from: https://doi.org/10.3390/rs10020313

Null, J. (2021) El Niño and La Niña years and intensities. Available at: https://ggweather.com/enso/oni.htm [Accessed 15th April 2021].

Pan, S., Pan, N., Tian, H., Friedlingstein, P., Sitch, S., Shi, H., et al. (2020) Evaluation of global terrestrial evapotranspiration using state-of-the-art approaches in remote sensing, machine learning and land surface modeling. *Hydrology and Earth System Sciences*, 24, 1485–1509. Available from: https://doi.org/10.5194/hess-24-1485-2020

Paredes-Trejo, F.J., Barbosa, H.A. & Kumar, T.V.L. (2017) Validating CHIRPS-based satellite precipitation estimates in northeast Brazil. *Journal of Arid Environments*, 139, 26-40. Available from: https://doi.org/10.1016/j.jaridenv.2016.12.009

Paschalis, A., Fatichi, S., Zscheischler, J., Ciais, P., Bahn, M., Boysen, L., et al. (2020) Rainfall manipulation experiments as simulated by terrestrial biosphere models: Where do we stand? *Global Change Biology*, 26, 3336–3355. Available from: https://doi.org/10.1111/gcb.15024

Pezzi, L.P. & Cavalcanti, I.F.A. (2001) The relative importance of ENSO and tropical Atlantic sea surface temperature anomalies for seasonal precipitation over South America: A numerical study. *Climate Dynamics*, 17, 205–212. Available from: https://doi.org/10.1007/s003820000104

Rossato, L., Alvalá, R.C.S., Marengo, J.A., Zeri, M., Cunha, A.P.M.A., Pires, L.B.M., et al. (2017) Impact of soil moisture on crop yields over Brazilian semiarid. *Frontiers in Environmental Science*, 5(73), 1–16. https://doi.org/10.3389/fenvs.2017.00073

Sá, L.D.A., Sambatti, S.B.M. & Galvao, G.P. (1998) Applying the Morlet wavelet in a study of variability of the level of Paraguay River at Ladario, MS. *Pesquisa Agropecuaria Brasileira*, 33, 1775–1785.

Schellekens, J., Dutra, E., Martínez-de la Torre, A., Balsamo, G., van Dijk, A., Sperna Weiland, F., et al. (2017) A global water resources ensemble of hydrological models: The eartH2Observe Tier-1 dataset. *Earth System Science Data*, 9, 389–413. Available from: https://doi.org/10.5194/essd-9-389-2017

Sellar, A.A., Walton, J., Jones, C.G., Wood, R., Abraham, N.L., Andrejczuk, M., et al. (2020) Implementation of U.K. earth system models for CMIP6. *Journal of Advances in Modeling Earth Systems*, 12(e2019MS001946), 1–27. https://doi.org/10.1029/2019MS001946

Sena, A., Freitas, C., Feitosa Souza, P., Alpino, T., Pedroso, M., Corvalan, C., et al. (2018) Drought in the semiarid region of Brazil: Exposure, vulnerabilities and health impacts from the perspectives of local actors. *PLoS Currents*, (1), 1–32. https://doi.org/10.1371/currents.dis.c226851ebd64290e619a4d1ed79c8639

Sepulcre-Canto, G., Horion, S., Singleton, A., Carrao, H. & Vogt, J. (2012) Development of a combined drought indicator to detect agricultural drought in Europe. *Natural Hazards and Earth System Science*, Available from: 12(11), 3519–3531. https://doi.org/10.5194/nhess-12-3519-2012

Simões, A.F., Kligerman, D.C., Rovere, E.L.L., Maroun, M.R., Barata, M. & Obermaier, M. (2010) Enhancing adaptive capacity to climate change: The case of smallholder farmers in the Brazilian semiarid region. *Environmental Science & Policy*, 13, 801–808. Available from: https://doi.org/10.1016/j.envsci.2010.08.005

Souza, A.G.S.S., Neto, A.R. & de Souza, L.L. (2021) Soil moisture-based index for agricultural drought assessment: SMADI application in Pernambuco State-Brazil. *Remote Sensing of Environment*, 252, 112124. Available from: https://doi.org/10.1016/j.rse.2020.112124

Svoboda, M.D. & Fuchs, B.A. (2017) *Handbook of drought indicators and indices, drought and water crises: Integrating science, management, and policy*, 2nd edition, Geneva: World Meteorological Organization (WMO) and Global Water Partnership (GWP). Available from: https://doi.org/10.1201/b22009

Thom, H.C.S. (1958) A note on the gamma distribution. *Monthly Weather Review*, 86, 117–122. Available from: https://doi.org/10.1175/1520-0493(1958)086⟨0117:anotgd⟩2.0.co;2

Tomasella, J., Silva Pinto Vieira, R.M., Barbosa, A.A., Rodriguez, D.A., Oliveira Santana, M.d. & Sestini, M.F. (2018) Desertification trends in the northeast of Brazil over the period 2000–2016. *International Journal of Applied Earth Observation and Geoinformation*, 73, 197–206. Available from: https://doi.org/10.1016/j.jag.2018.06.012

Torrence, C. & Compo, G.P. (1998) A practical guide to wavelet analysis. *Bulletin of the American Meteorological Society*, 79, 61–78. Available from: https://doi.org/10.1175/1520-0477(1998)079⟨0061:APGTWA⟩2.0.CO;2

Trenberth, K.E., Dai, A., van der Schrier, G., Jones, P.D., Barichivich, J., Briffa, K.R., et al. (2014) Global warming and changes in drought. *Nature Climate Change*, 4, 17–22. Available from: https://doi.org/10.1038/nclimate2067

Ukkola, A.M., de Kauwe, M.G., Pitman, A.J., Best, M.J., Abramowitz, G., Haverd, V., et al. (2016) Land surface models systematically overestimate the intensity, duration and magnitude of seasonal-scale evaporative droughts. *Environmental Research Letters*, 11, 104012. Available from: https://doi.org/10.1088/1748-9326/11/10/104012

van Loon, A.F. (2015) Hydrological drought explained. *Wiley Interdisciplinary Reviews: Water*, 2, 359–392. Available from: https://doi.org/10.1002/wat2.1085

Vicente-Serrano, S.M., Beguería, S. & López-Moreno, J.I. (2010) A multiscalar drought index sensitive to global warming: The standardized precipitation evapotranspiration index. *Journal of Climate*, 23(7), 1696–1718. https://doi.org/10.1175/2009JCLI2909.1

Walters, D.N., Williams, K.D., Boutle, I.A., Bushell, A.C., Edwards, J.M., Field, P.R., et al. (2014) The Met Office Unified Model Global Atmosphere 4.0 and JULES Global Land 4.0 configurations. *Geoscientific Model Development*, 7, 361–386. Available from: https://doi.org/10.5194/gmd-7-361-2014

Weedon, G.P., Balsamo, G., Bellouin, N., Gomes, S., Best, M.J. & Viterbo, P. (2014) The WFDEI meteorological forcing data set: WATCH Forcing Data methodology applied to ERA-Interim reanalysis data. *Water Resources Research*, 50, 7505–7514. Available from: https://doi.org/10.1002/2014WR015638

Wilhite, D.A. (2018) National drought management policy guidelines: A template for action. In: Wilhite, D. A., Pulwarty, R.S. (Eds.) *Drought and water crises: Integrating science, management, and policy*. Boca Raton, FL: CRC Press, pp. 55–94.

Wilhite, D.A., Sivakumar, M.V.K. & Pulwarty, R. (2014) Managing drought risk in a changing climate: The role of national drought policy. *Weather and Climate Extremes*, 3, 4–13. Available from: https://doi.org/10.1016/j.wace.2014.01.002

Wilks, D.S. (1995) *Statistical methods in the atmospheric sciences: An introduction*. San Diego, CA: Academic Press.

Xu, Y., Wang, L., Ross, K., Liu, C. & Berry, K. (2018) Standardized soil moisture index for drought monitoring based on soil moisture active passive observations and 36 years of North American land data assimilation system data: A case study in the Southeast United States. *Remote Sensing*, 10, 301. Available from: https://doi.org/10.3390/rs10020301

Yuan, J., Emura, K., Farnham, C. & Alam, M.A. (2018) Frequency analysis of annual maximum hourly precipitation and determination of best fit probability distribution for regions in Japan. *Urban Climate*, 24, 276–286. Available from: https://doi.org/10.1016/j.uclim.2017.07.008

Zeri, M., Alvalá, R.C.S., Carneiro, R., Cunha-Zeri, G., Costa, J.M., Spatafora, L.R., et al. (2018) Tools for communicating agricultural drought over the Brazilian semiarid using the soil moisture index. *Water*, 10, 1421. Available from: https://doi.org/10.3390/w10101421

Zeri, M., Costa, J.M., Urbano, D., Cuartas, L.A., Ivo, A., Marengo, J., et al. (2020) A soil moisture dataset over the Brazilian semiarid region. *Mendeley Data Version*, 2. Available from: https://doi.org/10.17632/xrk5rfcpvg.2

Zeri, M., Cunha-Zeri, G., Gois, G., Lyra, G.B. & Oliveira-Júnior, J.F. (2019) Exposure assessment of rainfall to interannual variability using the wavelet transform. *International Journal of Climatology*, 39, 568–578. Available from: https://doi.org/10.1002/joc.5812

SUPPORTING INFORMATION

Additional supporting information may be found online in the Supporting Information section at the end of the article.

How to cite this article: Zeri, M., Williams, K., Cunha, A.P.M.A., Cunha-Zeri, G., Vianna, M.S., Blyth, E.M., et al. (2022) Importance of including soil moisture in drought monitoring over the Brazilian semiarid region: An evaluation using the JULES model, in situ observations, and remote sensing. *Climate Resilience and Sustainability*, 1, e7. https://doi.org/10.1002/cli2.7